Generation of excited state potentials from photofragment spectral lines: Fano profiles in FNO

Moshe Shapiro
Department of Chemical Physics, The Weizmann Institute of Science, Rehovot, 76100, Israel

Hanna Reisler
Department of Chemistry, University of Southern California, Los Angeles, California 90089

(Received 12 January 1995; accepted 27 March 1995)

We develop a procedure to determine excited states potentials from photofragmentation data using *adiabatic energy curves*. The adiabatic curves, obtained from empirically derived *diabatic* channel potentials, are inverted to yield a polyatomic potential energy surface which is expressed as a piecewise collection of diatomic cuts. The procedure is applied to obtaining a two-dimensional potential of the FNO molecule in the S_1 excited state. The potential is more successful than available *ab initio* surfaces in reproducing the observed asymmetric (Fano) line shapes of the FNO $S_1 \leftarrow S_0$ state-specific photofragment yield spectra. © *1995 American Institute of Physics.*

I. INTRODUCTION

Usage of spectral line positions and line intensities in deriving the underlying potential(s) has been a longstanding goal of spectroscopy. In the context of diatomic spectroscopy, line positions can be inverted to yield the potential via the RKR procedure.[1] If the lines considered are such that the system is near harmonic, then Dunham expansion methods are also very effective.[2]

The problem becomes more complicated in the continuous part of the spectrum, where Dunham expansions cannot work. In diatomic molecules, scattering data[3] and the shape of the continuous spectrum[4] have been used, mainly in conjunction with the WKB approximation, to obtain potentials. Femtosecond transition state spectra were also used for potential inversion of diatomic potentials.[5] In triatomic and higher polyatomic molecules this cannot be easily done (see, however, Ref. 6), mainly because a good WKB theory for many-body systems does not exist.

In this paper we introduce a method that generates excited state potentials from photofragment spectral lines. We first use a parameter fitting procedure to convert the relative yields of production of various photofragments as a function of the photolysis frequency to a set of curves—the so-called ''adiabatic'' curves. We then apply a diatomic inversion procedure to each point in the adiabatic curves, thereby generating a polyatomic potential surface. The surfaces are obtained as a sequence of diatomiclike cuts. In this way the method extends diatomic methodology to polyatomic molecules, while circumventing the difficulties associated with the generation of polyatomic wave functions and energy levels.

Most previous theoretical studies of photodissociation were performed in the *forward* direction, in which the observables are calculated from the potential energy surfaces (PES).[7–9] The evaluation of PES's by such studies is made easier whenever the continuous absorption spectrum is characterized by the appearance of diffuse ''vibronic'' structures. Such diffuse lines are often assignable using physically meaningful (although approximate) quantum numbers. Their shapes were found to be very sensitive to the PES, especially in the Franck–Condon (FC) region.[9]

In a number of molecules the vibronic structures are due to the presence of shallow wells in the excited-state PES.[10,11] This is, in fact, the case for many XNO molecules (X=F, Cl, OH, CH_3O) (Ref. 11) which exhibit structured spectra resulting from shallow wells in the FC region, whose depths are of the order of magnitude of 0.1 eV.

Potential wells of such shallow depths are hard to obtain accurately by *ab initio* methods because their magnitude is often comparable to the accuracy of the calculations. Past dynamical calculations have shown that the spectral features of the XNO molecules are very sensitive to fine details of the PES.[11–14] Hence, the use of an experimentally based potential determination is especially warranted.

The rich data obtained in the $S_1 \leftarrow S_0$ photodissociation of FNO (Refs. 15 and 16) provides an excellent basis for application of our potential determination method. The $S_1 \leftarrow S_0$ FNO absorption spectrum shows a long NO stretch progression, as well as features assigned to bands that include contributions from F–N stretch and the FNO bend.[13,14] The line shapes in the state-selected spectra of FNO display[15,16] Fano-type[17] interferences: They arise from the simultaneous photoexcitation of the quasibound states supported by the shallow well residing to the left of a potential barrier, and continuum states of the steep repulsive part existing to the right of the barrier.[14]

The sense of asymmetry or ''shading'' (i.e., the sign of the Fano q parameter[17,18]) in some of the bands observed in the state-selected photofragment yield spectra [i.e., when monitoring different NO(v,J) product states] appears to be inordinately sensitive to the shape of the PES in the FC region. This shading is of particular importance, since it was shown experimentally that the state-specific shadings result in large variations in the NO $v=2/v=1$ branching ratios as the photolysis laser is scanned across the $S_1(200) \leftarrow S_0(000)$ absorption band.[16]

Existing *ab initio* S_1 surfaces have so far failed to reproduce the measured state-specific shadings,[19,20] even though many other experimental observations [e.g., the total FNO

 0021-9606/95/103(10)/4150/7/$6.00

absorption spectrum,[13,14] the existence of interference, [19] and the NO(v) rotational distributions and their dependence on excitation wavelength][13] were well reproduced. Thus, it is desirable to understand which features of the PES determine the shading of the line shapes and how to use this information to invert the data to obtain the potential.

The organization of this paper is as follows: In Sec. II we give a step-by-step explanation of the procedure by which the PES is generated from the experimental data. In Sec. III we apply this procedure to the FNO case. We summarize our conclusions in Sec. IV.

II. THE POTENTIAL DETERMINATION PROCEDURE

A. The photofragment spectrum

In order to best explain our inversion procedure we first describe the basic quantum theory underlying the calculations of the photofragment spectrum. In particular, we consider the photodissociation of a triatomic molecule ABC,

$$\mathrm{ABC}\xrightarrow{h\nu}\mathrm{A}+\mathrm{BC}.$$

The molecule, assumed initially in $|\,E_g\rangle$—a bound state on the ground potential W_{gr}—is excited by a light pulse of central frequency ν to a dissociative state characterized by a potential function W. Our aim is to extract W, assuming that W_{gr} is (at least partially) known and that we have measured the ''photofragment spectrum.''

The term photofragment spectrum, also known as ''photofragment mapping,''[21] ''state specific photofragment yield'' (PHOFRY) spectrum,[15] and ''photofragment excitation'' (PHOFEX) spectrum'',[22] is used to denote the relative photodissociation cross section to a single fragment state as a function of the photon energy. It is given as,[7,21]

$$\sigma(E,\mathbf{n}|E_g)=\frac{8\pi^3\nu}{c}|\langle\, E,\mathbf{n}^-\,|\mu_{\hat{\varepsilon}}|\,E_g\,\rangle|^2, \tag{2.1}$$

where E is the final continuum energy, E_g is the initial bound state energy, $\nu=(E-E_g)/h$, $\mu_{\hat{\varepsilon}}$ is the projection of the transition-dipole operator on the light's electric field direction, and $\mathbf{n}$ is a collective index for the internal (electronic, vibrational, rotational, etc.) quantum numbers of the fragments.

$|\,E,\mathbf{n}^-\,\rangle$ are (incoming) scattering eigenstates of the excited state Hamiltonian, $H=K+W$ (where K is the kinetic energy operator),

$$(E-H)|\,E,\mathbf{n}^-\,\rangle=0, \tag{2.2}$$

which go over in the long time limit to a product of a single fragment internal state $\phi_{\mathbf{n}}$ and a plane wave,

$$\langle\mathbf{R}|\,\mathbf{k}_{\mathbf{n}}\,\rangle\equiv\frac{1}{(2\pi\mathbf{k}_{\mathbf{n}})^{1/2}}\exp(i\mathbf{k}_{\mathbf{n}}\cdot\mathbf{R}), \tag{2.3}$$

describing the relative motion of the A-BC fragments,

$$|\,E,\mathbf{n}^-\,\rangle\xrightarrow{t\to\infty}|\,\phi_{\mathbf{n}}\,\rangle|\,\mathbf{k}_{\mathbf{n}}\,\rangle. \tag{2.4}$$

In what follows we assume that the state-selected photofragment spectrum has been measured and that, given the potential W, we have the ability to calculate it (using the artificial channel[8] or other methods[9]). Our task is to generate W, i.e., to invert the potential. We accomplish this by executing the following steps:

$$\textit{photofragment spectrum}\xrightarrow{1}\textit{channel potentials}\xrightarrow{2}\textit{adiabatic energy curves}\xrightarrow{3}\textit{the potential}.$$

In the following we describe this procedure in detail, starting from segment No. 3 and working our way back to segment No. 1.

B. From the adiabatic energy curves to the potential

For simplicity, we consider a two-dimensional (2D) model of the ABC triatomic described by the (Jacobi) coordinates, R, the A to B–C center-of-mass distance, and r, the B–C separation. In order to extract W it is useful to introduce the (somewhat modified) *hyperspherical* coordinates,[23] defined as

$$\rho=\left(R^2+\frac{m}{\mu}r^2\right)^{1/2},\quad s=\left(\frac{\mu}{m}\right)^{1/2}\rho\alpha, \tag{2.5}$$

where

$$\alpha=\tan^{-1}\left[\left(\frac{m}{\mu}\frac{r}{R}\right)^{1/2}\right], \tag{2.6}$$

with

$$m=\frac{m_{\mathrm{B}}m_{\mathrm{C}}}{m_{\mathrm{B}}+m_{\mathrm{C}}},\quad \mu=\frac{m_{\mathrm{A}}(m_{\mathrm{B}}+m_{\mathrm{C}})}{m_{\mathrm{A}}+m_{\mathrm{B}}+m_{\mathrm{C}}}. \tag{2.7}$$

ρ is a (non-mass-scaled) hyperradius, s is proportional to the length of the arc perpendicular to it (see Fig. 1), and α is the hyperangle tending this arc.

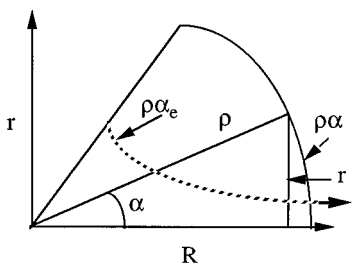

FIG. 1. Illustration of the hyperspherical coordinates. The hyperradius ρ, hyperangle α, and hyperarc $s(\rho)=\rho\alpha$ are defined in Eqs. (2.5)–(2.7). The dotted line refers to $s_\epsilon(\rho)$—the position of the minimum energy path for dissociation.

The reasons we have chosen to work with s and ρ, rather than with R and r is that $W(s,\rho)$, is always binding as a function of s. This follows, because the potential is bound between $\alpha=0$ and

$$\alpha=\tan^{-1}\left[\left(\frac{m_B(m_A+m_B+m_C)}{m_A m_C}\right)^{1/2}\right],$$

where the B–C and A–B distances, respectively, go to zero. If the system is nonreactive, W has a single minimum in s as $\rho\to\infty$. If the system is reactive, W has in that limit two minima, that of the reactants and that of the products.

The 2D Schrödinger equation for the nuclear motion in the hyperspherical coordinates assumes the form

$$\left(E+\frac{1}{2\mu}\frac{\partial^2}{\partial\rho^2}+\frac{1}{2m}\frac{\partial^2}{\partial s^2}-W(s,\rho)\right)\langle\rho|E,\mathbf{n}^-\rangle=0, \quad (2.8)$$

where atomic units ($\hbar=1$) are used throughout. The fact that W is binding in s allows us to first solve a bound state problem in s at each ρ value,

$$\left(\mathscr{E}_i(\rho)+\frac{1}{2m}\frac{d^2}{ds^2}-W(s,\rho)\right)\phi_i(s,\rho)=0, \quad (2.9)$$

obtaining a set of *adiabatic* eigenvalues $\mathscr{E}_i(\rho)$ and eigenfunctions $\phi_i(s,\rho)$. Equation (2.8) is then solved by expanding $\langle\rho|E,\mathbf{n}^-\rangle$ in this set,

$$\langle\rho|E,\mathbf{n}^-\rangle=\sum_i \phi_i(s,\rho)F_i^{\mathbf{n}}(\rho). \quad (2.10)$$

The $F_i^{\mathbf{n}}(\rho)$ coefficients satisfy a set of (coupled channels) equations, obtained by substituting Eq. (2.10) into Eq. (2.8),

$$\left[\left(E+\frac{1}{2\mu}\frac{d^2}{d\rho^2}\right)\cdot\mathbf{I}-\hat{\mathscr{E}}(\rho)-\mathbf{A}(\rho)\frac{d}{d\rho}-\mathbf{B}(\rho)\right]\mathbf{F}(\rho)=0, \quad (2.11)$$

where, $\mathbf{I}$ is the identity matrix,

$$\mathbf{F}(\rho)_{i,\mathbf{n}}\equiv F_i^{\mathbf{n}}(\rho) \quad (2.12)$$

is the matrix of expansion coefficients, and

$$\hat{\mathscr{E}}(\rho)_{i,j}\equiv\mathscr{E}_i(\rho)\,\delta_{i,j} \quad (2.13)$$

is a diagonal adiabatic eigenvalue matrix. The $\mathbf{A}(\rho)$ and $\mathbf{B}(\rho)$ matrices, defined as

$$\mathbf{A}(\rho)_{i,j}\equiv\frac{-1}{\mu}\int ds\,\phi_i^*(s,\rho)\frac{\partial}{\partial\rho}\phi_j(s,\rho) \quad (2.14)$$

and

$$\mathbf{B}(\rho)_{i,j}\equiv\frac{-1}{2\mu}\int ds\,\phi_i^*(s,\rho)\frac{\partial^2}{\partial\rho^2}\phi_j(s,\rho), \quad (2.15)$$

are the usual nonadiabatic coupling matrices.[24]

As shown later, once we know $\hat{\mathscr{E}}(\rho)$ we can use Eq. (2.9) to extract $W(s,\rho)$. This is possible because for every ρ value, Eq. (2.9) is a bound state problem in s. Such problems are routinely solved in the context of diatomic molecules through the Dunham expansion[2] or the semiclassical RKR procedure.[1] In diatomic molecules, in order to carry out such an inversion, prior information on the equilibrium separation (usually obtained from the rotational spectra) is needed. As explained later, in the present case this information is obtained from the ground state equilibrium configuration and the strength of the diffuse lines.

In order to clarify the procedure we look in greater detail at the 2×2 case, i.e., a case in which only two adiabatic curves are known. In this case strict RKR inversion is not possible, however a Dunham type expansion generating the first two terms is possible. Equivalently we can assume that $W(s,\rho)$ is parametrized as

$$W(s,\rho)=M(s,\rho)+V_{\min}(\rho), \quad (2.16)$$

where $M(s,\rho)$ is a Morse potential in s,

$$M(s,\rho)=D(\rho)(\exp\{-\beta(\rho)[s-s_e(\rho)]\}-1)^2, \quad (2.17)$$

depending parametrically on ρ.

Given two consecutive adiabatic eigenvalues $\mathscr{E}_v(\rho)$ and $\mathscr{E}_{v+1}(\rho)$, the fundamental frequency of the Morse oscillator, denoted as $\omega(\rho)$, is given as

$$\omega(\rho)=\frac{2(v+1)\mathscr{E}_v(\rho)-\Delta_v(\rho)(v+1/2)^2}{(v+1/2)(v+3/2)}, \quad (2.18)$$

where $\Delta_v(\rho)\equiv\mathscr{E}_{v+1}(\rho)-\mathscr{E}_v(\rho)$. The $D(\rho)$ and $\beta(\rho)$ parameters are then obtained as

$$D(\rho)=\frac{\omega(\rho)^2(v+1)}{2[\omega(\rho)-\Delta(\rho)]}, \quad \beta(\rho)=\omega(\rho)\left(\frac{\mu}{2D(\rho)}\right)^{1/2}. \quad (2.19)$$

Finally the ρ-dependent minimum potential of Eq. (2.16) is obtained as

$$V_{\min}(\rho)=\mathscr{E}_v(\rho)-(v+1/2)\omega(\rho)\left(1-\frac{\omega(\rho)}{4D(\rho)}(v+1/2)\right). \quad (2.20)$$

It is clear from Eq. (2.18) that the adiabatic eigenvalues are insensitive to the value of $s_e(\rho)$—the ρ-dependent equilibrium separation. In order to determine it we note that $s_e(\rho\to\infty)$ may be assumed known, since in that limit, $\rho\to R$ and $s\to r$, and,

$$M(s,\rho)\to v_{BC}(r), \quad (2.21)$$

where $v_{BC}(r)$ is the B–C diatomic potential. If we parametrize $v_{BC}(r)$ also as a Morse potential,

$$v_{BC}(r)=D(\exp[-\beta(r-r_e)]-1)^2, \quad (2.22)$$

then $s_e(\rho\to\infty)=r_e$.

We can also deduce (from the relative strengths of the diffuse lines—as explained later) the value of $s_e(\rho)$ at $\rho=\rho_g$, where

$$\rho_g=\left(R_g^2+\frac{m}{\mu}r_g^2\right)^{1/2}, \quad R_g=r_g(AB)+\frac{m_C}{m_B+m_C}r_g. \quad (2.23)$$

with $r_g(AB)$ and r_g being the ground state equilibrium separation between the A–B and B–C atoms, respectively.

This concluded the description of segment No. 3 in our inversion procedure.

C. From the matrix of channel potentials to the adiabatic energy curves

We now outline the way the adiabatic curves are obtained. This is done from the matrix of (diabatic) channel potentials which are extracted from the experimental data.

The diabatic representation arises in the usual way[25] by transforming away the first derivative matrix in Eq. (2.11). Introducing a matrix **U** satisfying,

$$\mathbf{A}\cdot\mathbf{U}+\frac{1}{\mu}\frac{d\mathbf{U}}{d\rho}=0, \tag{2.24}$$

we operate with $\mathbf{U^{-1}}$ on Eq. (2.11), to obtain a *diabatic* set of equations,

$$\left[\left(E+\frac{1}{2\mu}\frac{d^2}{d\rho^2}\right)\cdot\mathbf{I}-\mathbf{V}(\rho)\right]\mathbf{G}(\rho)=0, \tag{2.25}$$

where

$$\mathbf{V}(\rho)=\mathbf{U}^{-1}\cdot[\hat{\mathscr{E}}(\rho)+\mathbf{B}(\rho)]\cdot\mathbf{U} \tag{2.26}$$

and

$$\mathbf{G}(\rho)=\mathbf{U}^{-1}\cdot\mathbf{F}(\rho). \tag{2.27}$$

Assuming that the $\mathbf{V}(\rho)$ matrix has been extracted from the experimental data (in a procedure to be described in detail in the next subsection), we can diagonalize $\mathbf{V}(\boldsymbol{\rho})$ to obtain

$$\hat{\mathscr{E}}'(\rho)=\mathbf{X}^{-1}(\rho)\cdot\mathbf{V}(\rho)\cdot\mathbf{X}(\rho). \tag{2.28}$$

Operating with $\mathbf{X}^{-1}(\rho)$ on Eq. (2.25) leads to a set of equations identical in form to our original adiabatic equations [Eq. (2.11)],

$$\left[\left(E+\frac{1}{2\mu}\frac{d^2}{d\rho^2}\right)\cdot\mathbf{I}-\hat{\mathscr{E}}'(\rho)-\mathbf{A}'(\rho)\frac{d}{d\rho}-\mathbf{B}'(\rho)\right]\mathbf{F}'(\rho)=0. \tag{2.29}$$

with $\hat{\mathscr{E}}'(\rho)$ given by Eq. (2.28), $\mathbf{A}'(\rho)$ given as,

$$\mathbf{A}'(\rho)=\frac{1}{\mu}\mathbf{X}^{-1}(\rho)\frac{d}{d\rho}\mathbf{X}(\rho), \tag{2.30}$$

and

$$\mathbf{B}'(\rho)=\frac{1}{2\mu}\mathbf{X}^{-1}(\rho)\frac{d^2}{d\rho^2}\mathbf{X}(\rho). \tag{2.31}$$

Because of the identity between Eqs. (2.11) and (2.29), we equate between $\hat{\mathscr{E}}'(\rho)$ and $\hat{\mathscr{E}}(\rho)$. Strictly speaking, these two entities are equal only for an infinite basis set. Assuming this identity, we are thus able to calculate the set of adiabatic curves $\hat{\mathscr{E}}(\rho)$, from which W is obtained, given the $\mathbf{V}(\rho)$ matrix.

In Sec. III, we outline the way the matrix of channel potentials is obtained from the experimental data. For the sake of clarity, we specialize the description to the case actually tried—that of the FNO molecule.

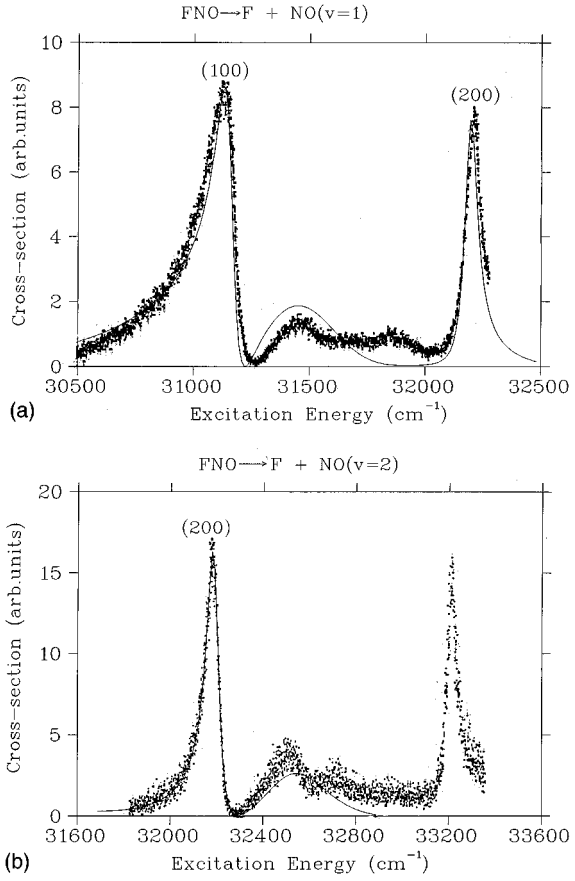

FIG. 2. Experimental (scattered dots) and theoretical (solid line) photofragment yield spectra. Panels (a) and (b) show the the spectra obtained by monitoring the NO($v=1,J$) and NO($v=2,J$) channels, respectively.

III. INVERSION OF THE FNO EXPERIMENTAL PHOTOFRAGMENT SPECTRUM

A. Review of the FNO experimental data

The main input data were the NO($v=1$) and NO ($v=2$) state-specific photofragment yield spectra obtained following $S_1\leftarrow S_0$ excitation. The experimental spectra of NO($v=1,2$; $J=29.5$) used in this work are shown in Fig. 2. Similar spectra were obtained for other rotational levels.[26] Note especially the asymmetric appearance of the lines (Fano line shapes[17]) at $\sim$31 000 cm^{-1} [assigned in the figure as (100) (Ref. 15)] and $\sim$32 100 cm^{-1} [assigned as (200) Ref. 15)]. Of particular importance is the observation that, when exciting in the region of the (200) resonance, the sense of the asymmetry (i.e., whether the peak appears to the red or to the blue of the dip—the so called ''shading'') of the Fano lineshapes in the two monitored NO vibrational levels is reversed: The NO($v=1$) component is shaded to the blue, whereas the NO($v=2$) component is shaded to the red. This brings about the observed[15] large variation in the NO ($v=2$)/NO($v=1$) ratio when the excitation frequency is scanned across the (200) resonance. In general, when n quanta of NO stretch in FNO are excited, red-shaded lines are associated with monitoring the NO($v=n$) channel (the

''elastic'' channel), while blue-shaded lined are observed when monitoring NO($v=n-1$), i.e., the ''inelastic'' channel.

Such reversal in shading has not been reproduced in the dynamical calculations performed so far using existing *ab initio* PES's.[19,14] The observation of Fano profiles in photodissociation of polyatomic molecules and especially a reversal of the shading of the line shape is rare (see, however, Ref. 10). Thus understanding how such phenomenon arises is interesting in its own right.

In contrast to the experimental results, the bending progression cannot be obtained in our 2D calculations. However, since the experimentally observed Fano profiles are best resolved for the (n00) resonances (which have no bending excitation), we believe that simulation of this part of the spectrum is important to the understanding of the dynamics. It has been shown before that the NO stretch is largely uncoupled from the bend, while the bend and F–NO stretch are strongly coupled.[14,27,28] Moreover, the reported NO rotational distributions associated with the ''elastic'' and ''inelastic'' channels following excitation of each (n00) resonance are similar. Both are bell shaped, peaking at $\sim J=30.5$ with a width of ~ 10 rotational levels. Thus the measured relative line intensities obtained when monitoring NO(v) rotational levels near the peak of the rotational distribution are approximately equal to the ratio of the NO channels associated with $v=n$ and $v=n-1$.

B. The diabatic channel potentials

The channel potential for the ground state was parametrized as a Morse potential,

$$V_g(\rho)=D_g\{\exp[-\beta_g(\rho-\rho_g)]-1\}^2+V_g^{\min}. \tag{3.1}$$

The excited diabatic channel potentials were parametrized in a flexible way as a sum of a Morse potential and a ''soft'' step potential,

$$V_{i,i}(\rho)=D_i\{\exp[-\beta_i(\rho-\rho_i)]-1\}^2+D_i + \frac{a_{d,i}}{1+\exp[b_{d,i}(\rho-\rho_{d,i})]}, \quad i=1,2. \tag{3.2}$$

In this equation, $i=1,2$ denote curves correlating to the NO($v=1$) and NO($v=2$) fragments, respectively. ρ_i is the Morse equilibrium distance, β_i is the Morse exponent, D_i is the depth of the (shallow) well, $\rho_{d,i}$ determines the location of the step, and $a_{d,i}$ and $b_{d,i}$ determine, respectively, the height and steepness of the step. The off-diagonal potential was parametrized as a Gaussian function of the form

$$V_{1,2}=a_{1,2}\exp[-b_{1,2}(\rho-\rho_{1,2})^2]. \tag{3.3}$$

In the fitting reported here only the two ($v=1$ and $v=2$) NO channels photofragment spectra, shown in Figs. 2(a) and 2(b) (reproduced from Refs. 13 and 26), were used. The fitting was made easier by the high correlation between the aforementioned potential parameters and the important spectral features. These correlations are listed in the following.

(i) D_i and $a_{d,i}$, which determine the overall energy location of the $V_{i,i}$ curves, are directly correlated to the center frequency of the (100) and (200) resonances.

(ii) ρ_i, and $\rho_{d,i}$ (together with D_i, and $a_{d,i}$) determine the well depths, heights, and widths of the diabatic barriers potentials. They are directly correlated to the energetic widths of the resonances.

(iii) The off-diagonal potential parameters $a_{1,2}$, $b_{1,2}$, and $\rho_{1,2}$, and mainly the $a_{1,2}$ parameter, which determines the strength of the interaction, correlate to the degree of nonadiabaticity (or inelasticity) during the fragmentation process. This, in turn, is reflected in the NO ($v=2$)/NO($v=1$)/NO($v=0$) product branching ratios. We found that the data is mainly sensitive to the form of the off-diagonal potential in the exit channel regions, i.e., in the barrier region and beyond.

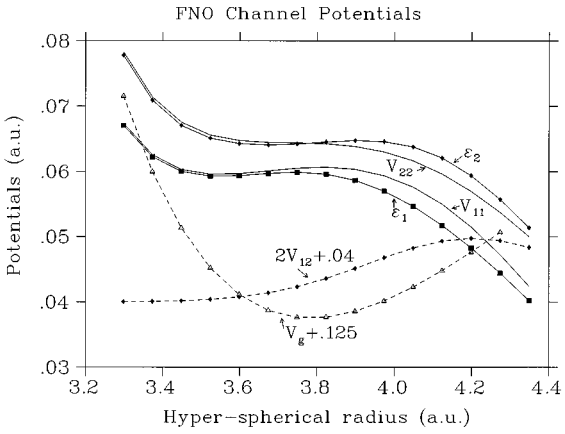

FIG. 3. The diabatic channel potentials V_{11} and V_{22} giving rise to the theoretical line shapes of Fig. 2. Shown also are $\mathscr{E}_1$ and $\mathscr{E}_2$—the (adiabatic) eigenvalues of the 2×2 diabatic potential matrix—as well as the coupling potentials V_{12} and the ground-state potential V_g.

TABLE I. Potential parameters (in a.u.).

Parameter	Numerical value	Parameter	Numerical value	Parameter	Numerical value
D_1	1.43×10^{-2}	β_1	2.5	ρ_1	3.5118
D_2	1.14×10^{-2}	β_2	2.4	ρ_2	3.5958
D_g	$8.746\,559\,2\times10^{-2}$	β_g	1.0	ρ_g	3.8582
$a_{d,1}$	6.19×10^{-2}	$b_{d,1}$	4.8	$\rho_{d,1}$	4.3722
$a_{d,2}$	5.61×10^{-2}	$b_{d,2}$	4.3	$\rho_{d,2}$	4.4103
$a_{1,2}$	4.87×10^{-3}	$b_{1,2}$	7.0	$\rho_{1,2}$	4.2013
r_e(NO)	2.18	$s_e(\rho_1)$	2.3		
ω(NO)	$8.474\,773\,8\times10^{-3}$	$\omega(\rho_1)$	$4.761\,364\,85\times10^{-3}$		

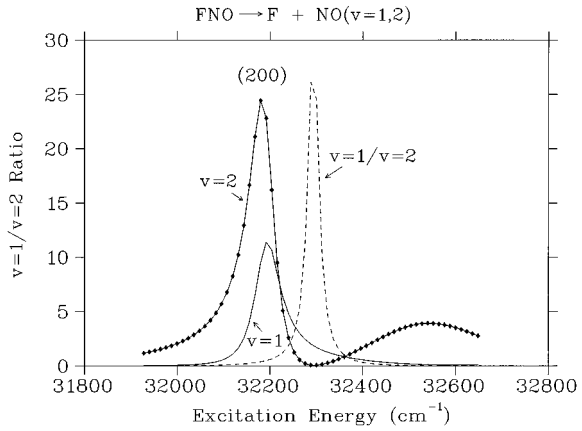

FIG. 4. The NO($v=1$) and NO($v=2$) photofragment line shapes in the vicinity of the (200) resonance and the ratio between them.

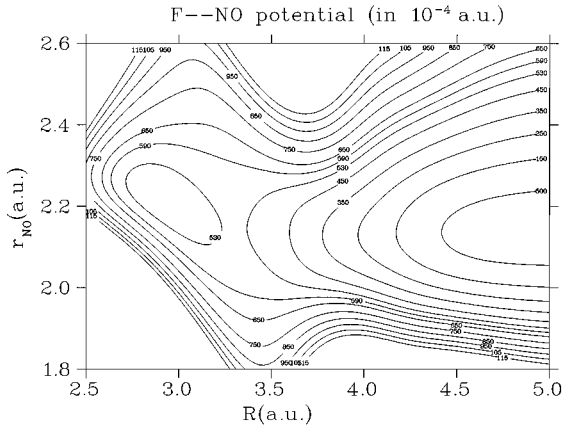

FIG. 5. The 2D FNO potential derived from the diabatic matrix of Fig. 3. The equipotential curves are given in units of 10^{-4} a.u.

(iv) The relative positions of the ground and excited state wells, given by ρ_g, ρ_i, in conjunction with the barrier positions determined by $\rho_{d,i}$, govern the interference leading to the formation of the asymmetric Fano line shapes. The shadings, indeed the very existence of asymmetry in the line shapes, are the most sensitive attributes to the potential parameters since they depend on the phase. Even a slight change in these parameters can lead to a cancellation or a reversal of the asymmetry. Hence, the data being comprised of asymmetric line shapes are especially useful in the potential inversion.

(v) The (200)/(100) peak intensity ratio is mainly affected by the relative position of r_g of Eq. (3.1) and ρ_i of Eq. (3.2) as well as that of $s_e(\rho_i)$ of Eq. (2.17), and the NO fragment equilibrium position r_e of Eq. (2.22). The latter quantity controls the vibrational Franck–Condon (FC) factors.

Using the ''best'' channel potentials (depicted in Fig. 3), whose parameters (given in Table I) are obtained by the aforementioned procedure, we have computed [with the ACM (Ref. 8)] the photofragmentation line shapes. The theoretical results, displayed in Figs. 2(a) and 2(b), are in remarkably good agreement with the experimental results.[13,26] We see that the computed line shapes reproduce quantitatively well all the important line shapes features: their asymmetries, shadings, positions, widths and [NO($v=2$)/NO($v=1$)] ratios. It is interesting to note that the satellite peaks located $\sim 400\ \mathrm{cm}^{-1}$ to the blue of the main peak which were attributed to bending vibrations[13,26] are also well reproduced by the present 2D model. They originate from an additional quasibound level lying very close to the top of the barrier. (Similar assignments were reached by Cotting *et al.*,[19] who used an *ab initio* 2D PES.) In addition to the aforementioned, as can be seen in Figs. 2(a) and 2(b), the experiments show a second small satellite absent from the present theoretical line shapes, whose origin must therefore be exclusively due to the bending motion.

In Fig. 4 we present the NO($v=2$), NO($v=1$) photofragment line shapes and their ratio in the (200) resonance region. The difference in the shading of the two line shapes results in a sharp dependence of their ratio on the excitation energy, which allows to ''dial in'' essentially any desired ratio. Here, again, good agreement with the results observed experimentally is obtained.[13,26]

C. The FNO potential

The 2×2 diabatic channel potentials matrix **V,** derived as explained in Sec. III B, was used to construct a 2D potential surface of FNO by following Eqs. (2.17)–(2.20), and (2.27)–(2.29). The results are shown in Fig. 5 and compared to the *ab initio* calculations of Suter *et al.*[14] displayed in Fig. 6. The experimental data used here are sensitive predominantly to the region near the minimum energy path. It is less sensitive to regions much beyond that path which have no effect on the experimental observables.

It is difficult to directly compare the 2D surface generated here with the 2D *ab initio* potential at a fixed bending angle since our potential is really an average over the bending motion of the true 3D potential. Nevertheless, a close examination of the two potentials in the Franck–Condon region reveal greater similarities than apparent in the small scale drawing of Fig. 6. For example, although this may not be surmised from Fig. 6 itself, the *ab initio* potential possesses a shallow minimum in the F–NO exit channel similar to that of our empirically derived potential.

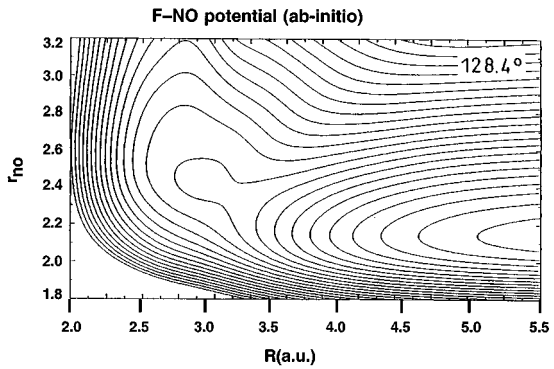

FIG. 6. The *ab initio* FNO potential of Ref. 14. The equipotential curves are spaced by 0.25 eV.

IV. DISCUSSION AND CONCLUSIONS

We described here a potential inversion procedure of photofragment data. The procedure is an extension to polyatomic molecules of diatomic energy levels based inversions. The key concept in this extension is the use of adiabatic energy *curves*. The polyatomic PES is generated as a piecewise set of diatomic potentials. We have applied this inversion procedure to obtaining 2D PES of FNO. The potential we have obtained reproduces the observed asymmetric line shapes, their shadings, and the vibrational distribution in the region of the (200) resonance with remarkable accuracy.

The FNO inversion allowed us to test the general procedure and to gain insight into the correlation between PES parameters and spectral features. The main experimental observations and their correlation to the PES parameters are the following.

1. The FNO molecule displays asymmetric line shapes (i.e. Fano profiles) in the state-selected photofragment spectra resulting from interference in the pre-barrier and post-barrier regions. Occasionally, a secondary peak appears to the blue of a red-shaded absorption feature. This peak is due to the existence of an F–NO stretch level near the top of the barrier.

2. The shadings in the state-selected photofragment spectra are determined by the location of the (small) wells and barriers of the excited-state adiabatic energy curves relative to the ground-state potential. As observed experimentally, the two channels correlating to the NO($v=1$) and NO ($v=2$) states posses line shapes of opposite shadings, which in turn lead to large variations in the branching ratios with excitation energy. Due to their inordinate sensitivity to the parameters of the PES discussed earlier, the asymmetry shadings enable a very precise determination of the location of the adiabatic wells and barriers.

3. The intensity ratios of the photofragment line shapes are determined to a large extent by the NO FC factors and the strength of the off-diagonal potential. The latter acts mainly near the top and in the exit region of the barrier.

ACKNOWLEDGMENTS

H.R. would like to thank the Weizmann Institute for financial support during her visit, the U.S. National Science Foundation for supporting this research, and S.A. Reid and J.T. Brandon for many stimulating discussions and for providing the experimental data. M.S. acknowledges support by the Israel Science Foundation of the Israel Academy of Sciences.

[1] J. R. Rydberg, Z. Phys. **73** 376 (1931); O. Klein, *ibid.* **76**, 226 (1932).
[2] G. Herzberg, *Molecular Spectra and Molecular Structure. I. Spectra of Diatomic Molecules* (Van Nostrand Reinhold, New York, 1950).
[3] R. B. Gerber, M. Shapiro, U. Buck, and J. Schleusener, Phys. Rev. Lett. **41**, 236 (1978).
[4] H. Blum, J. Lindner, and E. Tiemann, J. Chem. Phys. **93**, 4556 (1990); S. H. Schaefer, D. Bender, and E. Tiemann Chem. Phys. **89**, 65 (1984); Chem. Phys. Lett. **92**, 273 (1982)
[5] A. H. Zewail Faraday Disc. Chem. Soc. **91**, 207 (1991); M. Gruebele, G. Roberts, M. Dantus, R. M. Bowman, and A. H. Zewail, Chem. Phys. Lett. **166**, 459 (1990); R.B. Bernstein and A.H. Zewail, *ibid.* **170**, 321 (1990); M. H. M. Janssen, R. M. Bowman, and A. H. Zewail, *ibid.* **172**, 99 (1990); M. Gruebele and A. H. Zewail, J. Chem. Phys. **98**, 883 (1993).
[6] T.-S. Ho and H. Rabitz, J. Phys. Chem. **97**, 13 447 (1993).
[7] M. Shapiro, Isr. J. Chem. **11**, 691 (1973).
[8] M. Shapiro, J. Chem. Phys. **56**, 2582 (1972).
[9] See, R. Schinke, *Photodissociation Dynamics* (Cambridge University Press, Cambridge, 1992).
[10] J. A. Beswick and M. Shapiro, Chem. Phys. **64**, 333 (1982).
[11] J. R. Huber and R. Schinke, J. Phys. Chem. **97**, 3463 (1993).
[12] D. Soelter, H.-J. Werner, M. v. Dirke, A. Untch, A. Vegiri, and R. Schinke, J. Chem. Phys. **97**, 3357 (1992).
[13] A. Ogai, J. T. Brandon, H. Reisler, H. U. Suter, J. R. Huber, M. v. Dirke, and R. Schinke, J. Chem. Phys. **96**, 6643 (1992).
[14] H. U. Suter, J. R. Huber, M. v. Dirke, A. Untch, and R. Schinke, J. Chem. Phys. **96**, 6729 (1992).
[15] J. T. Brandon, S. A. Reid, D. C. Robie, and H. Reisler, J. Chem. Phys. **97**, 5246 (1992).
[16] S. A. Reid, J. T. Brandon, and H. Reisler, J. Phys. Chem. **97**, 540 (1993).
[17] U. Fano Phys. Rev. **124**, 1866 (1961).
[18] R. D. Levine, *Quantum Mechanics of Molecular Rate Processes* (Clarendon, Oxford, England, 1969).
[19] R. Cotting, J. R. Huber, and V. Engel, J. Chem. Phys. **100**, 1040 (1994).
[20] R. Schinke, (private communication).
[21] M. Shapiro, Chem. Phys. Lett. **46**, 442 (1977); **81**, 521 (1981); M. Shapiro, J. Phys. Chem. **90**, 3644 (1986).
[22] W. H. Green, Jr., C. B. Moore, and W. F. Poli, Annu. Rev. Phys. Chem. **43**, 307 (1992).
[23] L. M. Delves, Nucl. Phys. **20**, 275 (1960); A. Kuppermann, J. A. Kaye, and J. P. Dwyer, Chem. Phys. Lett. **74**, 257 (1980); J. Romelt, *ibid.* **74**, 263 (1980); G. Hauke, J. Manz, and J. Romelt, J. Chem. Phys. **73**, 5040 (1980).
[24] See, J. H. Van Vleck, Rev. Mod. Phys. **23**, 213 (1951); W. R. Thorson, J. Chem. Phys. **34**, 1744 (1961); **39**, 1431 (1963); R. D. Levine and B. R. Johnson, Chem. Phys. Lett. **13**, 168 (1972); R. D. Levine, M. Shapiro, and B. R. Johnson, J. Chem. Phys. **52**, 1755 (1970).
[25] F. T. Smith, Phys. Rev. **179**, 111 (1969); Z. H. Top and M. Baer, J. Chem. Phys. **66**, 1363 (1977).
[26] J. T. Brandon, S. A. Reid, and H. Reisler (unpublished).
[27] L. H. Jones, L. B. Asprey, and R. R. Ryan, J. Chem. Phys. **47**, 337 (1967).
[28] S. C. Foster and L. H. Jones, J. Mol. Spectrosc. **103**, 176 (1984).